PRZEGLĄD ELEKTROTECHNICZNY

Ukazuje się od 1919 roku 10'14

Organ Stowarzyszenia Elektryków Polskich • Wydawnictwo SIGMA-NOT Sp. z o.o.

Jacek F. GIERAS

University of Technology and Life Sciences, Bydgoszcz, Poland

PM Generator for Novel Architecture of Wind Turbines

Abstract*. The paper deals with a permanent magnet (PM) generator for novel architecture of wind turbines. The proposed wind turbine consists of a number of integrated lower-poer individual generators. The individual generators can be arranged in a rectangular matrix, hexagon or in a circle. The paper discusses sizing procedure for this type of generators, electromagnetic calculations including the finite element method (FEM) simulation, performance characteristics and advantages of this type of wind generator. As an example, a PM brushless generator with concentrated non-overlap stator coils has been considered.*

Streszczenie. *Artykuł dotyczy prądnicy bezszczotkowej o magnesach trwałych do nowej architektury turbin wiatrowych. Proponowana turbina wiatrowa składa się z pewnej liczby zintegrowanych jednostek o mniejszej mocy. Poszczególne prądnice mogą być zestawione w matrycę prostokątną, hexagon lub wpisane w okrąg. W artykule omówiono procedurę wymiarowania tego typu prądnic, obliczenia elektromagnetyczne, w tym rownież za pomocą metody elementów skończonych (MES), charakterystyki pracy oraz zalety. Jako przykład, została rozważona prądnica bezszczotkowa o magnesach trwałych z uzwojeniem stojana o cewkach o parametrach skupionych i rozpiętości jednej podziałki żłobkowej.*
Nowa architektura prądnicy do turbin wiatrowych o magnesach trwałych

Keywords: wind turbine, novel architecture, permanent magnet generator, electromagnetic calculations, performance characteristics.
Słowa kluczowe: turbiną wiatrowa, nowa architektura, prądnica o magnesach trwałych, obliczenia elektromagnetyczne, parametry.

doi:10.12915/pe.2014.10.01

Introduction

Wind turbine generators convert wind energy into electrical energy with the aid of mechanical rotation of a bladed rotor hub. In the past, most wind turbines have utilized heavy gearboxes to convert slow, powerful rotor hub rotation into much faster rotation of a driveshaft connected mechanically to the electrical generator. Gearboxes typically require regular maintenance (lubrication), and account for substantial energy losses, thus reducing the overall efficiency of the wind turbine system. Many newer wind turbines instead utilize direct-drive generators [4] that eschew gearboxes in favour of a large-diameter generator rotor attached directly to the turbine rotor hub.

To achieve the necessary rotor linear speeds, direct-drive generator rotors may be several meters in diameter. Although direct-drive generators avoid many of the challenges associated with gearbox-driven generators, the extremely large diameter of most direct-drive generator rotors adds significant weight and cost to direct-drive wind turbines [1,4]. In addition, the air gap of a large diameter generator must typically be increased to allow for proportionally greater radial translation due to rotor hub deflection. Increased air gap deteriorates the generator performance. Most direct drive generators include heavy support structures designed to minimize the rotor hub deflection. This additional mass contributes significantly to the total material, production, and assembly costs of the wind turbine.

The advantages of distributed generation from renewable power sources (such as ambient wind) have long been recognized. Despite some of the challenges associated with power distribution, control and delivery, many successful recent studies have demonstrated the viability of the approach [4,5,6].

This work demonstrates the technical viability of the new concept of distributed wind energy power generation by integration of smaller units into large wind turbine system.

Technical approach

The proposed distributed wind generator can consist of any number of integrated smaller individual generators (Fig. 1). Fig. 2a shows 19 integrated generators arranged hexagonally and Fig. 3b shows also 19 generators arranged circularly.

The individual generator units can also be assembled to form a rectangle with m rows and n columns creating a matrix of $m \times n$ generators.

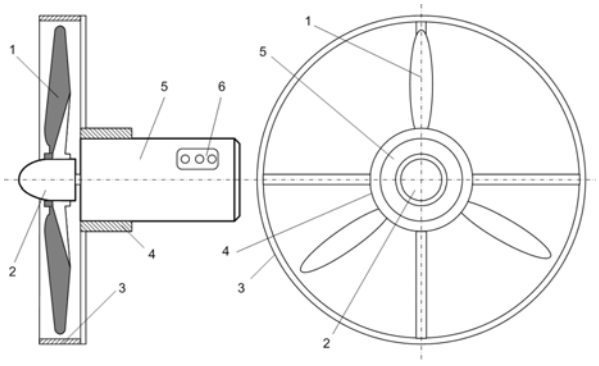

Fig. 1. Construction of a single integrated module of wind turbine generator: 1 – propeller, 2 – propeller hub, 3 – rim, 4 – bushing, 5 – electric generator with built-in rectifier, 6 – terminal board.

The power of a single integrated generator can typically range from 20 to 250 kW. Using, say, 20 generator units, the total power of the windmill is 0.4 to 5.0 MW. For example, an electric generator rated at 25 kW has the stator core outer diameter of about 0.45 m, and the stack length of

about 0.3 m. Other power ratings, sizes and numbers of individual generator units are, of course, also possible.

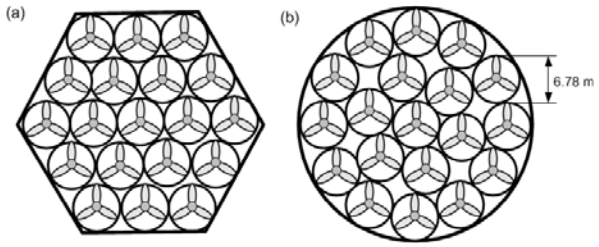

Fig. 2. Novel architecture of electric generators showing an arrangement of 19 units (modules): (a) hexagonal; (b) circular.

Sizing procedure

The maximum value of the Betz limit [5] for wind turbines is $c_p \approx 0.593$. A more practical value including frictional losses is $c_p = 0.4$.

For a total power of a wind turbine P_t = 500 kW, the number of individual generator N_t = 19, electric efficiency (generator and power electronics converter) η_{el} = 0.885, Betz limit c_p = 0.4, incoming air wind speed $v \approx 15$ m/s, rotational speed of the rotor n_r = 132 rpm, air density, ρ_{air} = 1.22 kg/m^3, and number of blades n_b = 4, the electric output power P_{el}, mechanical (shaft) power P_m, rotor swept area, A, and diameter d of rotor blades of an individual generator are, respectively:

(1) $$P_{el} = \frac{P_t}{N_t} = \frac{500}{19} = 26.316 \quad \text{kW}$$

(2) $$P_m = \frac{P_{el}}{\eta_{el}} = \frac{26.315}{0.885} = 29.735 \quad \text{kW}$$

(3) $$A = \frac{P_m}{0.5 c_p \rho_{air} v^3} = \frac{29735}{0.5 \times 0.4 \times 1.22 \times 132^3} = 36.11 \quad \text{m}^2$$

(4) $$d = 2\sqrt{\frac{A}{\pi}} = 2\sqrt{\frac{36.11}{\pi}} = 6.78 \quad \text{m}$$

The rotational speed of the rotor n_r = 132/60 = 2.2 rev/s and the tip speed of the rotor

(5) $$v_{tip} = 2\pi n_r \frac{d}{2} = 2\pi \times 2.2 \frac{6.78}{2} = 36.86 \quad \frac{\text{m}}{\text{s}}$$

The rotor tip speed is well below the 80 m/s mechanical integrity limit [5]. Also, the tip speed ratio

(6) $$\text{TSR} = \frac{v_{tip}}{v} = \frac{36.86}{15} = 3.124$$

is very close to the optimal tip speed ratio [5], i.e.,

(7) $$\lambda_{opt} = \frac{4\pi}{n_b} = \frac{4\pi}{4} = 3.14 \approx \text{TSR}$$

The inner diameter D_{1in} of the stator of the electric generator and its stack length L are linked with the electric output power P_{el} with the following equation [2,3]:

(8) $$P_{el} = \frac{\pi}{6\sqrt{2}} \frac{1}{\varepsilon} n_r k_{w1} D_{1in}^3 L J_{\max} B_g a_p k_{fill} (k_y^2 - 1) \eta_{el} \cos\varphi$$

Assuming the stator stack inner diameter D_{1in} = 0.3544 m, stator stack length L = 0.31 m, EMF-to-voltage ratio ε = 1.08, winding factor k_{w1} = 0.945, maximum current density in the stator winding J_{max} = 2.3×10^6 A/m^2, air gap magnetic flux density B_g = 0.7 T, number of the stator winding parallel paths a_p = 2, stator slot fill factor k_{fill} = 0.444, stator yoke diameter-to-inner diameter k_y =1.293, generator efficiency η_g = 0.934 and power factor $\cos\varphi$ = 0.95, the electric power calculated on the basis of eqn (8) is P_{el} = 26.4 kW, almost the same as that given by eqn (1). The results given by eqns (1) to (8) can then be used in the electromagnetic calculations of the electric generator.

Electromagnetic design

Permanent magnet (PM) brushless generator has been selected as the most efficient and compact electrical machine [1]. The electromagnetic calculations have been performed using both analytical method and the finite element method (FEM) analysis. Table 1 shows the geometry and dimensions of the magnetic circuit, Table 2 shows the stator winding parameters and Table 3 shows the rated (nominal) parameters of the PM brushless generator for novel architecture of the wind turbine.

Table 1. Geometry, magnetic circuit dimensions and mass of active components.

Number of stator slots	54
Number of poles	60
Stator outer diameter, mm	468.0
Stator inner diameter, mm	354.4
Rotor outer diameter, mm	352.0
Rotor inner diameter	320.0
Radial thickness of air gap (clearance), mm	1.2
Length of the stator and rotor stack, mm	310.0
Stator slot depth, mm	52.0
Stator slot opening, mm	2.0
Width of stator tooth, mm	8.0
Radial thickness of stator yoke, mm	4.8
Radial thickness of rotor yoke, mm	6.0
PM radial thickness, mm	10.0
Circumferential width of PM, mm	17.4
Mass of copper winding, kg	53.73
Mass of stator core, kg	72.85
Mass of rotor core, kg	14.25
Mass of PMs, kg	26.42
Total mass of active components, kg	167.3
Rotor moment of inertia excluding shaft, kgm^2	0.3787

Table 2. Stator winding parameters

Number of phases	3
Connection	Wye
Number of turns per coil	18
Number of turns per phase	162
Number of layers in slots	2
Number of strands in hand	18
Number of parallel paths	2
Coil span (throw)	1 slot
Winding factor for fundamental harmonic	0.9452
Conductor	AWG 20
Conductor diameter, mm	0.8128
Stator slot fill factor	0.4439
Resistance per phase at 20°C, Ω	0.0995
Resistance per phase at 100°C (hot machine), Ω	0.1308
d-axis synchronous inductance, mH	5.0686
q-axis synchronous inductance, mH	5.503

Table 3. Rated (nominal) parameters of PM brushless generator.

AC line-to-line voltage, V	400
Rotational speed, rpm	132
Frequency of stator (armature) current, Hz	66
Load angle δ, elec. degree	25
Shaft torque, Nm	2113.8
Shaft mechanical power, kW	29.22
Electrical output power, kW	27.3
Electromagnetic (air gap) power, kW	28.0
Generator efficiency, %	93.44
Solid state converter efficiency, %	94.71
Power factor $\cos\phi$	0.92
Stator *d*-axis current, A	1.32
Stator *q*-axis current, A	42.86
Stator current, A rms	42.88
Stator current density. A/mm^2	2.3
EMF constant, Vs/rad	38.193

The stator and rotor core have been stacked with M19 silicon steel laminations. The rotor field excitation system consists of 60 pieces (2*p* = 60) of *Vacodym 510* NdFeB PMs (Vacuumschmelze, Hanau, Germany) with remanent magnetic flux density B_r = 1.38 T and coercivity H_c = 955 kA/m at 20°C ambient temperature. The cost of PMs is significant and estimated as approximately US$3170 (US$120 per 1 kg of sintered NdFeB).

In the design calculation, the following temperatures have been assumed: ambient temperature = 20°C, winding temperature = 100°C and PM temperature = 60°C. The stator winding has been designed as *fractional slot per pole per phase winding* called also *non-overlap concentrated coil winding*. For this type of winding [1]

$$\frac{N_c}{\gcd(N_c,2p)} = k\,m_1 \tag{9}$$

where N_c = 54 = total number of coils in three-phase winding, 2*p* = 60 = number of poles, *k* = 1,2,3,.., and *gcd* is the greatest common divisor of N_c and 2*p*. For this machine *gcd* (54,60) = 6 and $k \times m_1$ = 9, so the stator winding is feasible. The stator overhangs are very short, i.e., the total axial length of the stator with end turns is approximately 326 mm. The mean length of turn is 666 mm.

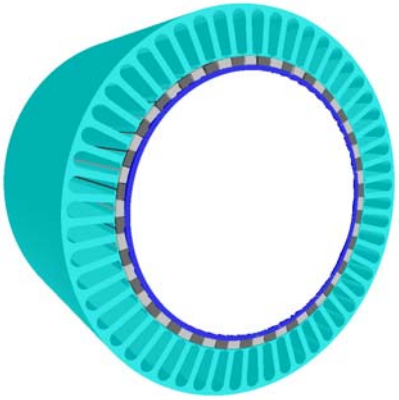

Fig. 3. Computer generated 3D image of the PM brushless generator. Only active components, i.e., the stator core, rotor core and PMs have been shown.

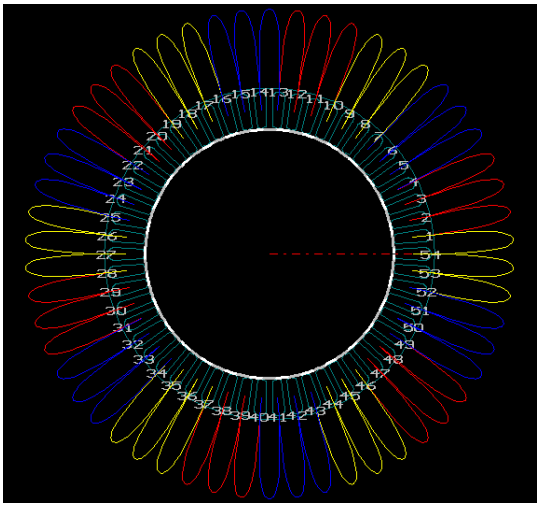

Fig. 4. Three-phase winding consisting of non-overlap coils with one slot coil span (54 slots, 3/10 slots per pole per phase).

The 3D image of the generator is shown in Fig. 3 and the stator winding diagram in Fig 4.

To reduce the winding losses and increase the efficiency, a low value of the stator current density 2.3 A/mm^2 has been chosen (Table 3). The electric efficiency η_{el} = 0.885 is the product of the generator efficiency and solid state converter efficiency (Table 3).

The magnetic flux lines and magnetic flux density distribution in the cross section of the generator as obtained from the 2D FEM is shown in Fig. 5. The open-circuit air gap normal component of the magnetic flux density averaged over one pole pitch is 0.758 T. The same magnetic flux density obtained from the 2D FEM is 0.803 T. The magnetic flux density in the stator teeth does not exceed 2.12 T, while the magnetic flux density in the stator yoke is about 1.82 T.

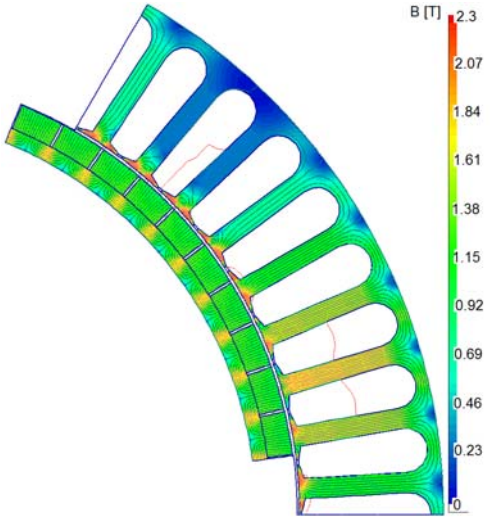

Fig. 5. Magnetic flux lines and magnetic flux density distribution in a 10-pole segment of the generator as obtained from the 2D FEM

Performance characteristics

The steady-state performance characteristics as obtained from the electromagnetic calculations are shown in Figs 6 to 11.

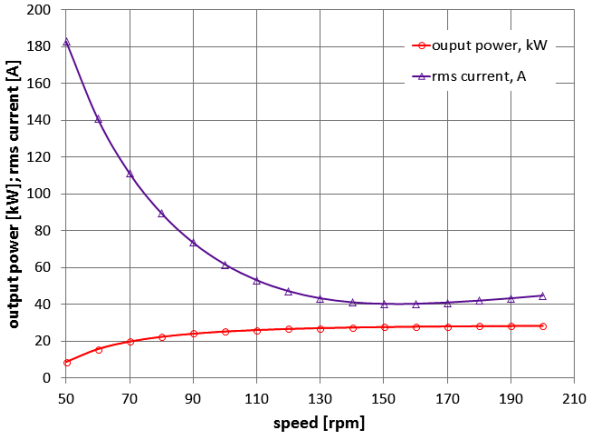

Fig.6. Output electrical power and rms current versus speed at constant load angle δ = 25° and line-to-line voltage 400 V

The generator can deliver the rated (nominal) power when its rotational speed is minimum 110 rpm (Fig. 6). If the speed is below 90 rpm the generator should be disconnected or operate with reduced load, because at speed lower than 90 rpm the current density takes high values (Fig. 7). The efficiency exceeds 90% when the rotational speed is greater than 90 rpm (Fig. 8). The higher the rotational speed, the lower propeller torque is required (Fig. 9). The total losses (stator winding, core and windage losses) are about 2 kW at rated load.

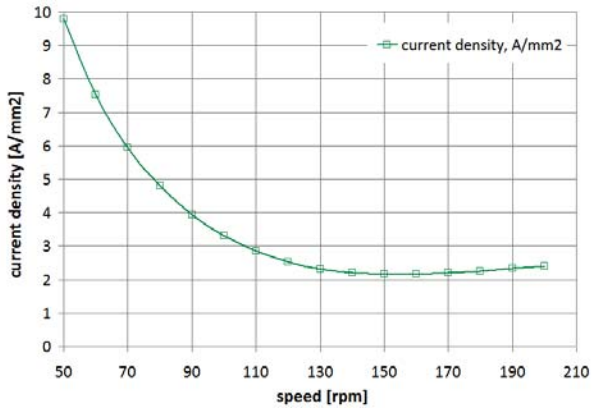

Fig. 7. Stator winding current density versus speed at constant load load angle δ = 25° and line-to-line voltage 400 V

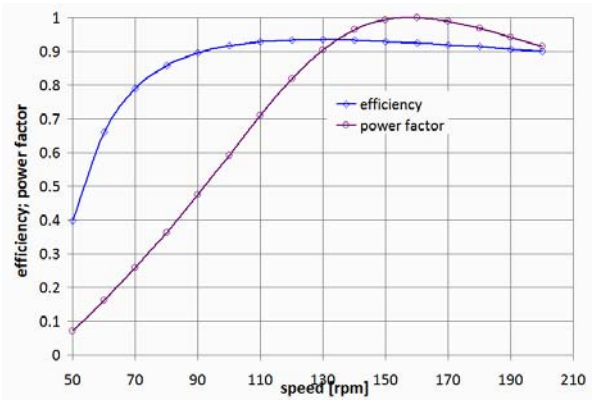

Fig. 8. Efficiency and power factor cosφ versus speed at constant load load angle δ = 25° and line-to-line voltage 400 V

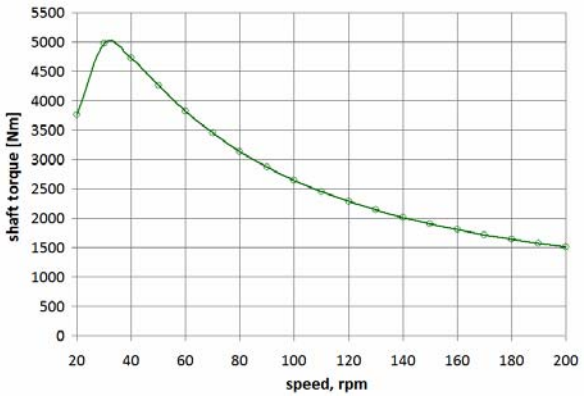

Fig. 9. Shaft torque versus speed at constant load load angle δ = 25° and line-to-line voltage 400 V

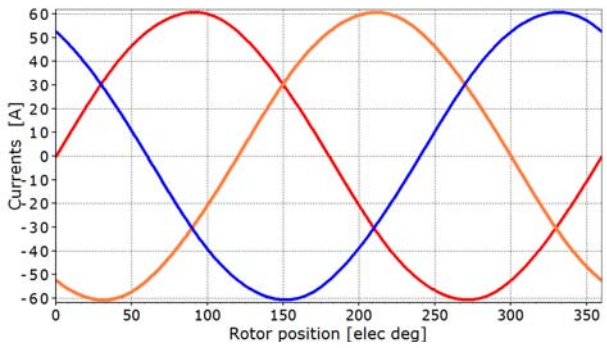

Fig. 10. Armature winding phase currents at 400 V terminal voltage and rated load

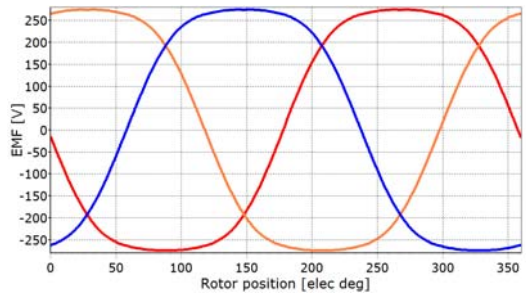

Fig. 11. EMFs induced in armature windings at 400 V terminal voltage and rated load.

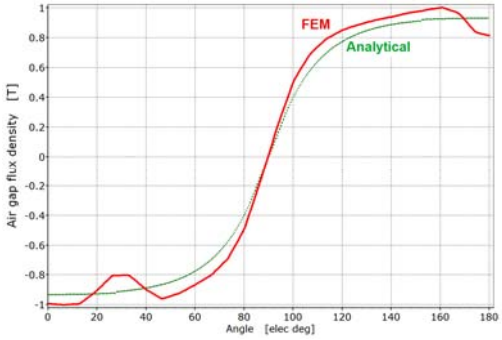

Fig. 12. Comparison of normal components of air gap magnetic flux density distribution obtained from analytical calculations and 2D FEM simulation.

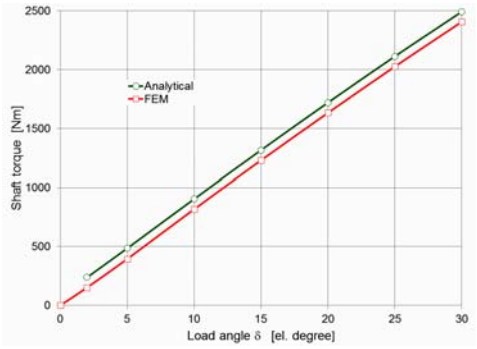

Fig. 13. Comparison of shaft torque versus load angle calculated analytically and with the aid of 2D FEM (132 rpm, 400 V).

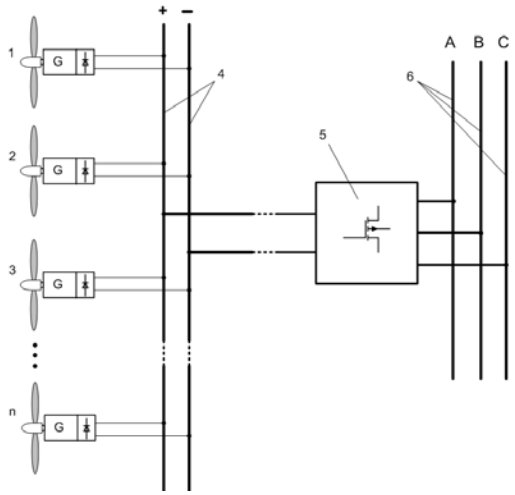

Fig. 14. Electrical connection of distributed wind generator to the electric power distribution network: 1,2,3,…n – plurality of wind electric generators integrated with propellers and rectifiers, 4 – DC bus bars, 5 – VVVF solid state inverter, 6 – 3-phase power distribution network.

Armature winding phase currents for generator operating without rectifier are sinusoidal (Fig. 10). EMFs induced in armature windings are balanced, but contain the 5^{th} and 7^{th} harmonics (Fig. 11).

Analytical calculations have been verified with the 2D FEM (Figs 12 and 13). The shaft torque versus load angle δ obtained from analytical calculations is slightly higher than that obtained from the 2D FEM.

Electrical connection and rectifier operation

An exemplary electrical connection of distributed wind generators to power distribution network is shown in Fig. 13. Individuals generators (modules) are integrated with propellers and solid state rectifiers. To avoid problems with synchronization, the DC output terminals of rectifiers are connected in parallel on a DC bus bars. The AC distribution network can be either a 3-phase or single-phase network.

To keep constant output frequency, the solid state inverter 5 (Fig. 14) must be a variable voltage variable frequency (VVVF) inverter.

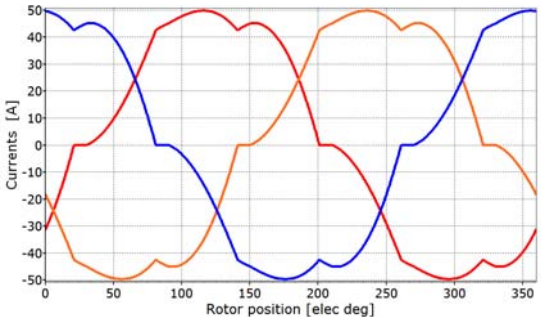

Fig. 15. Phase currents at rectifier operation (18.8 kW DC output power, 400 V DC, 47.2 A rms rectifier current).

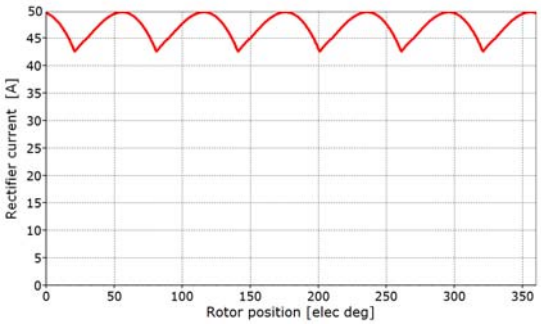

Fig. 16. Rectifier current 47.2 A rms at 18.8 kW DC output power, 400 V DC.

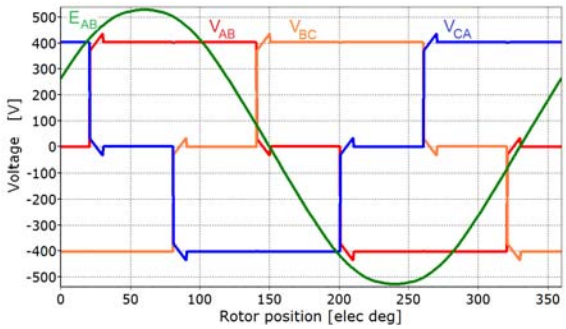

Fig. 17. Line-to-line voltage at armature winding terminals and line-to-line EMF at rectifier operation (18.8 kW DC output power, 400 V DC, 47.2 A rms rectifier current).

Phase current, rectifier current and voltage waveforms at rectifier operation are plotted in Figs. 14, 15, and 16. All diagrams refer to a single generator unit integrated with a solid state passive rectifier.

Conclusions

An innovative concept of a novel wind power generation system has been demonstrated. This system consists of a certain number of smaller, identically-sized individual wind generator units, each based on the PM brushless machine technology.

The distributed modular design allows to manufacture only one "common" size, one rating generator unit and then to assembly a wind generation system of any required electrical output power.

In addition, unlike conventional single-rotor wind generators, there is an increased reliability and redundancy of the proposed wind generation system, i.e., if one or more units fail, the wind generator still will be operating and generating electricity.

Smaller generator units produce lower acoustic emissions due to their lower individual noise level. The brushless PM generators allow smooth operation allowing proper ridethrough control during intermittent power transients.

Finally, the modular design of the individual wind generators leads to reduced manufacturing costs due to the unification of common parts.

REFERENCES

[1] Gieras, J. F., *Permanent Magnet Motor Technology: Design and Applications*, 3rd edition, Taylor & Francis, Boca Raton – London – New York, 2012.

[2] Gieras, J.G., New Applications of Synchronous Generators, *Przeglad Elektrotechniczny (Electrical Review)*, vol. 88, No 9a, 2012, 150-157.

[3] Gieras, J.F., Multimegawatt Synchronous Generators for Airborne Applications: a Review, *IEMDC 2013*, Chicago, IL, USA, 2013, 653-660.

[4] Polinder, H., van der Pijl, F. F. A., de Vilder, G.-J., Tavner, P. J., "Comparison of Direct-Drive and Geared Generator Concepts for Wind Turbines," *IEEE Transactions on Energy Conversion*, Vol. 21, No. 3, Sep. 2006, 725-733,

[5] Ragheb, M., Ragheb, A. M., Wind Turbines Theory – The Betz Equation and Optimal Rotor Tip Sped Ratio, Chpt. 2 in *Fundamental and Advanced Topics in Wind Power*, Ed. by Rupp Carriveau, InTech, Jul. 5 2011, DOI: 10.5772/731, 19-38.

[6] Sobczyk, T.J, Mazgaj, W., Szular, Z, Wegiel, T., Energy Conversion in Small Water Plants with Variable Speed PM Generator, *Archives of Elec. Eng.*, vol. 60, No 2, 2011, 159-168.

***Author**: Prof. Jacek F. Gieras, PhD, DSc, IEEE Fellow, University of Technology and Life Sciences, Department of Electrical Engineering, Al. S. Kaliskiego 7, 85-796 Bydgoszcz, Poland, E-mail: jacek.gieras@utp.edu.pl*